UCRL-19451

C. 2

RECEIVED
LAWRENCE
RADIATION LABORATORY

MAR 13 1970

LIBRARY AND
DOCUMENTS SECTION

NUCLEON-NUCLEON TRIPLE-SCATTERING PARAMETERS 510-670 MeV

Pamela Hansen Surko
(Ph. D. Thesis)

January 15, 1970

AEC Contract No. W-7405-eng-48

TWO-WEEK LOAN COPY

This is a Library Circulating Copy which may be borrowed for two weeks. For a personal retention copy, call Tech. Info. Division, Ext. 5545

LAWRENCE RADIATION LABORATORY
UNIVERSITY of CALIFORNIA BERKELEY

UCRL-19451

DISCLAIMER

This document was prepared as an account of work sponsored by the United States Government. While this document is believed to contain correct information, neither the United States Government nor any agency thereof, nor the Regents of the University of California, nor any of their employees, makes any warranty, express or implied, or assumes any legal responsibility for the accuracy, completeness, or usefulness of any information, apparatus, product, or process disclosed, or represents that its use would not infringe privately owned rights. Reference herein to any specific commercial product, process, or service by its trade name, trademark, manufacturer, or otherwise, does not necessarily constitute or imply its endorsement, recommendation, or favoring by the United States Government or any agency thereof, or the Regents of the University of California. The views and opinions of authors expressed herein do not necessarily state or reflect those of the United States Government or any agency thereof or the Regents of the University of California.

NUCLEON–NUCLEON TRIPLE–SCATTERING PARAMETERS 510–670 MeV

Contents

Abstract iv

I. Introduction 1

II. Theory

A. Constituents of the Elastic Scattering Amplitude . . 3

B. Symmetry Properties of the Amplitudes 4

C. Experimental Observables 4

III. Experimental Method and Apparatus

A. Introduction 8

B. First Scatter 8

C. Polarized Beam 10

D. Second Scatter 11

E. Third Scatter 12

F. Fast Electronics 13

G. Data Acquisition 14

IV. Data Analysis

A. Pattern Recognition 15

B. Kinematic Reconstruction 16

C. Asymmetry–Determination 16

D. Depolarization Parameter Calculation 18

V. Results

A. Depolarization in the Proton–Proton System 19

B. Transfer Depolarization in the Neutron–Proton System 20

C. Contributions to Errors 21

D. Conclusion 22

Acknowledgments 24

Appendix 1 25

References 26

Tables 28

Figure Captions 30

Figures 32

NUCLEON-NUCLEON TRIPLE-SCATTERING PARAMETERS 510-670 MeV

Pamela Hansen Surko

Lawrence Radiation Laboratory
University of California
Berkeley, California

January 15, 1970

ABSTRACT

The values of the Wolfenstein depolarization parameter D are reported at 670, 600, and 520 MeV for the pp interaction, over the CM angular range 30°–120°. The transfer depolarization parameter D^t has been measured at 600 and 525 MeV in the free np system, over the range 65°–180° CM.

Five points are measured at each energy, with statistical accuracy averaging about $\pm$ .1 for D_{pp} and $\pm$ .3 for D^t_{np}. D^{pp} is between 1/2 and 1 at forward scattering angles and drops toward zero at angles greater than 90° CM. It remains positive. D^t_{np} is small and positive at measured angles less than 90° and also at 180°. There is an indication of a possible negative value between 90° and 180°.

Predictions of various phase-shift solutions are compared to the data.

A polarized neutron/proton beam was produced by elastically scattering the beam of the Berkeley 184" Cyclotron off deuterium/hydrogen. The polarized beam was elastically scattered off hydrogen and the polarization of the recoil proton analyzed in a carbon-slab and magnetostrictive-wire-chamber array.

I. INTRODUCTION

The "medium-energy" region of nucleon-nucleon interactions between pion production threshold and higher energies handled by Regge theory seems to be a most difficult one for theoreticians and parameterizers alike.

At low energies, phase shift analysis is practical and informative. A phase shift analysis makes good use of the smooth variation of parameters with angle and energy. Unitarity is built in. There seem to be reasonable ways (OPE) to guess the behavior of the high ℓ phase shifts. However, the number of parameters increases with energy, doubling as the first inelastic channel opens up. In the energy region of this work, 500 MeV - 670 MeV, phase shift analyses require over fifty parameters. Going to higher and higher ℓ for parameterization of higher energy data does not look practical at the present time.

Puzikov, Ryndin and Smorodinskii[7] proposed in 1957 that for these higher energies, parameterization directly in terms of the scalar amplitudes of the elastic scattering matrix element would be preferable. As higher energies are studied, the number of parameters would not increase, and with appropriate selections of experiments, the matrix element could be determined uniquely. With this technique, experiments measuring two spins are essential. Schumacher and Bethe[8] showed that for each isospin state, all five complex amplitudes, relative to a common phase, could be determined for a given angle and energy by measuring the differential cross-section and ten second order polarization tensors. This type of investigation has become possible with the advent of good polarized targets and polarized beams.

The state of our knowledge of the nucleon-nucleon interaction is

improving. MacGregor, Arndt, and Wright[9] have been able to make an energy dependent phase shift analysis from 0 - 450 MeV, with the I = 1 scattering matrix uniquely and accurately determined over the range. The I = 0 phases are well determined near 142, 210 and 425 MeV, where triple scattering data was available. They are ambiguous at other energies, even though energy-independent phase shifts seemed good fits to the data.

The state of our understanding does not seem to have kept pace with the state of our knowledge, however. In 1960, Maurice Goldhaber commented,

> "There are few problems in modern theoretical physics which have attracted more attention than that of trying to determine the fundamental interaction between two nucleons. It is also true that scarcely ever has the world of physics owed so little to so many. In general, in surveying the field, one is oppressed by the unbelievable confusion and conflict that exists. It is hard to believe that many of the authors are talking about the same problem or, in fact, that they know what the problem is."

Advances in meson field theory in recent years make the outlook considerably less bleak, but probably no one would claim any startling improvement. Most theories require the exchange of the π meson to dominate the long range attractive interaction, with various combinations of ω, ρ, η, and a J = 0, I = 0 meson or a two-pion s wave exchange to take care of the short range repulsion and the intermediate range interactions. Theories require from two to fifteen parameters, and many fit the phase shifts reasonably well.

II. THEORY

A. Constituents of the Elastic Scattering Amplitude

Although the two-nucleon problem has been with us for nearly 40 years discussions of the possible constituents of the matrix element as restricted by invariance principles come from the 1950's, for example, Wolfenstein and Ashkin (1952)[1] and Dalitz (1952).[2]

Physical quantities available for construction of matrix element terms are $\hat{\sigma}^1$, $\hat{\sigma}^2$, $\hat{K}$, $\hat{P}$, and $\hat{N}$, where $\hat{\sigma}^1$ and $\hat{\sigma}^2$ are the spins of the nucleons, and $\hat{K}$, $\hat{P}$, and $\hat{N}$ are momentum vectors related to center of mass momentum vectors. If k is the incoming momentum vector, and k' that for the outgoing particle,

$$\begin{aligned} \hat{P} &= \widehat{k + k'} \\ \hat{K} &= \widehat{k' - k} \\ \hat{N} &= \widehat{k \times k'} \end{aligned} \tag{1.1}$$

For nonrelativistic energies, $\hat{P}$ is the outgoing momentum in the laboratory system.

The matrix element must be rotationally invariant, therefore scalar or pseudoscalar. It must be invariant under parity transformation ($\hat{\sigma} \to \hat{\sigma}$, $\vec{p} \to -\vec{p}$) and time reversal ($\hat{\sigma} \to -\hat{\sigma}$, $\hat{N} \to -\hat{N}$, $\hat{P} \to -\hat{P}$, $\hat{K} \to \hat{K}$). The extended Pauli principle requires invariance under the interchange of labels 1 and 2 for identical particles. The most general possible matrix element with these restrictions is

$$\begin{aligned} M = a + ic\,[(\hat{\sigma}^1+\hat{\sigma}^2).\hat{N}] + m(\hat{N}.\hat{\sigma}^1\,\hat{\sigma}^2.N) + g[\hat{P}.\hat{\sigma}^1\hat{\sigma}^2.\hat{P} + \hat{K}.\hat{\sigma}^1\hat{\sigma}^2.\hat{K}] \\ + h\,[\hat{P}.\hat{\sigma}^1\hat{\sigma}^2.\hat{P} - \hat{K}.\hat{\sigma}^1\hat{\sigma}^2.\hat{K}] \end{aligned} \tag{1.2}$$

in the notation of Moravcsik.[3] The complex scalar amplitudes a, c, m, g, and h are functions of scattering angle and energy, and have isoscalar and isotriplet parts. Below the inelastic threshold, imaginary and real parts

of each amplitude are related through unitarity. Above the threshold for pion production there are 20 independent functions of angle and energy with one phase arbitrary. Therefore, nineteen experiments performed at all angles and energies would seem to be the minimum requirement for determination of the matrix element. However, experimental observables are bilinear functions of the scalar amplitudes, and additional measurements are required for a unique determination.

B. Symmetry Properties of the Amplitudes

The extended Pauli principle requires well defined symmetry under interchange of fermions in a given isospin state. We may write

$$M_I\,(p', p) = (-1)^I\,\underline{P}\,(1, 2)\,M_I\,(-p', p) = (-1)^I M_I\,(p', -p)\,\underline{P}\,(1, 2). \tag{1.3}$$

Here p and p' are the CM momenta of the incident and scattered particles, $\underline{P}\,(1, 2) = 1/2\,(1 + \sigma_1\sigma_2)$ is the operator which permutes spins, and I indicates the isospin state. From the above and from equation (1.2) we may obtain[6, 3]

$$\begin{aligned} c_I(\theta) &= (-1)^{I+1} c_I(\pi-\theta) \\ h_I(\theta) &= (-1)^{I+1} h_I(\pi-\theta) \\ a_I(\theta)+m_I(\theta) &= (-1)^I[a_I(\pi-\theta)+m_I(\pi-\theta)] \\ 1/2\,[a_I(\theta)-m_I(\theta)] &= (-1)^I g_I(\pi-\theta) \end{aligned} \tag{1.4}$$

Thus, if all the scalar amplitudes were known in the CM angular region $0 < \theta < \pi/2$, the scattering amplitude would be determined.

C. Experimental Observables

Experimentally, the initial and final states are mixtures of various spin states. It is convenient to use the density matrix formulation.[25]

The density matrix is defined as

$$\sum_{\alpha=1}^{N} \psi_i^{\alpha} \psi_j^{\alpha *} w(\alpha) = \rho_{ij}$$

where the ψ's are the 4-component spin wave functions of the two nucleon system, α denotes the various states and the $w(\alpha)$'s are weight functions.

Remembering[4] that for an operator O

$$< O > = \frac{Tr(O\rho)}{Tr\rho}$$

and $\rho^f = M\rho^i M^*$, and $I_o = \frac{Tr\rho^f}{Tr\rho^i} \equiv 1/4\ Tr\rho^f$ where I_o is the unpolarized differential cross-section, we may write

$$I_o < \sigma_\mu^{1f} \sigma_\nu^{2f};\ \sigma_\tau^{1i}\ \sigma_\omega^{2i} > = 1/4\ Tr(\sigma_\mu^{1f}\ \sigma_\nu^{2f} M\ \sigma_\tau^{1i}\ \sigma_\omega^{2i} M^*) \qquad (1.5)$$

where the states are now labeled by the measured components of the spins of the individual nucleons. The left hand side is the expectation value of the $\sigma_\mu^1\ \sigma_\nu^2$ final state when the initial density matrix $\sigma_\tau^1\ \sigma_\omega^2$ is given. For convenience the abbreviation $< \mu\nu; \tau\omega >$ will be used for $I_o < \sigma_\mu^{1f}\ \sigma_\nu^{2f}; \sigma_\tau^{1i}\ \sigma_\omega^{2i} >$. Greek indices run over 0, 1, 2, 3 where zero indicates the subscripted spin is unmeasured, and 1, 2, 3 label the measured components $\hat{P}$, $\hat{K}$ and $\hat{N}$ respectively. Of the 256 possible measurements, most are either zero or related to others through the invariance properties of the scattering amplitude.

The notation of Wolfenstein[5] seems to be universally accepted among experimenters. Wolfenstein defined five experimentally convenient parameters in the laboratory system which describe how various components of the spin change when a scatter occurs. The D, R, R', A and A' experiments are shown in Fig. 1. Each involves the measurement of one spin component in the initial state and a spin component of the same nucleon in the final state. Five other "transfer" Wolfenstein parameters are similarly defined, for the cases where the relevant spin component of the recoil particle is

measured. This parameterization is especially convenient because each spin component is parallel or perpendicular to the laboratory momentum vector of the nucleon.

As pictured in Fig. 1, in the nonrelativistic limit the five parameters are related to the previously discussed expectation values as follows:

$$
\begin{aligned}
I_o D &= (N, 0;\ N, 0) \\
I_o R &= (K, 0;\ K, 0)\cos\theta/2 + (K, 0;\ P, 0)\sin\theta/2 \\
I_o A &= (K, 0;\ K, 0)\cos\theta/2 - (K, 0;\ P, 0)\sin\theta/2 \\
I_o R' &= (P, 0;\ K, 0)\cos\theta/2 + (P, 0;\ P, 0)\sin\theta/2 \\
I_o A' &= (P, 0;\ P, 0)\cos\theta/2 - (P, 0;\ K, 0)\sin\theta/2
\end{aligned}
\tag{1.6}
$$

The relationship of the expectation values to the various amplitudes may be calculated.

$$
\begin{aligned}
(0, 0;\ 0, 0) &= |a|^2+2|c|^2+|m|^2+2|g|^2+2|h|^2 \\
(N, 0;\ N, 0) &= |a|^2+2|c|^2+|m|^2-2|g|^2-2|h|^2 \\
(K, 0;\ K, 0) &= |a|^2-|m|^2-4\ \mathrm{Re}\ gh^* \\
(K, 0;\ P, 0) &= -(P, 0;\ K, 0) = -2\ \mathrm{Re}[c(a-m)^*] \\
(P, 0;\ P, 0) &= |a|^2-|m|^2+4\ \mathrm{Re}\ gh^*
\end{aligned}
\tag{1.7}
$$

In addition, the amplitudes making up the transfer Wolfenstein parameters are

$$
\begin{aligned}
(0, N;\ N, 0) &= +2[\mathrm{Re}\ a^*m + |c|^2+|g|^2-|h|^2] \\
(0, K;\ K, 0) &= 2\ \mathrm{Re}[(a+m)g^* - (a-m)h^*] \\
(0, K;\ P, 0) &= -(0, P;\ K, 0) = -4\ \mathrm{Re}\ cg^* \\
(0, P;\ P, 0) &= 2\ \mathrm{Re}[(a+m)g^* + (a-m)h^*]
\end{aligned}
\tag{1.8}
$$

We may calculate from equations (1.6), (1.7), and (1.8)

$$
\begin{aligned}
I_o(1-D) &= 4(|g|^2+|h|^2) \\
I_o(1-D^t) &= 4|h|^2+a^2+m^2-2\ \mathrm{Re}a^*m
\end{aligned}
\tag{1.9}
$$

Measurements of D and D^t are not enough to determine single scalar amplitudes, but if C_{NN}((N, N; 0, 0) or (0, 0; N, N)) is also measured, we may determine

$$
\begin{aligned}
|g|^2 &= 1/8\ I_o\ (1 + D^t - D - C_{NN}) \\
|h|^2 &= 1/8\ I_o\ (1 - D^t - D + C_{NN}) \\
|a+m|^2 &= 1/2\ I_o\ (1 - D^t + D - C_{NN}) \\
1/4\,|a-m|^2 - |c|^2 &= 1/8\ I_o\ (1 + D^t + D + C_{NN})
\end{aligned}
\tag{1.10}
$$

These combinations of measurements give only the squares of scalar amplitudes, so the measurements of the rotation parameters R, R', A and A', which are functions of interference terms are very valuable. The other way to get terms linear in the various amplitudes is to perform experiments at small angles where interference between nuclear and Coulomb amplitudes is appreciable.

III. EXPERIMENTAL METHOD AND APPARATUS

A. Introduction

To measure a Wolfenstein parameter, a polarization must be known in both the initial and final states. In the initial state, a polarized beam may be made by scattering an unpolarized beam at an angle and energy where previous knowledge shows the polarization is high, or if experiments are limited to those with only polarized protons in the initial state, a polarized target may be used.

In the triple-scattering experiments reported here, a scattering was used to achieve an initial-state polarized neutron or proton beam. The second scatter is the one to be studied, and a third scatter off carbon was used to analyze the polarization of the recoil proton.

B. First Scatter

The layout of the experimental apparatus is shown in Fig. 2. The 184-Inch Cyclotron proton beam of 735 $\pm$ 5 MeV kinetic energy was extracted into the proton cave, focused by quadrupole Q1, then deflected by bending magnets B1 and B2 to achieve a laboratory scattering angle γ. Magnet B2 was mounted on rails and a pivot so that both positive and corresponding negative angles could be used. Scattering angles of $\pm 15^{\circ}$, $\pm 22^{\circ}$, and $\pm 28^{\circ}$ were used, to make polarized proton beams of 670 MeV, 600 MeV, and 520 MeV, respectively. Polarized neutron beams of 600 MeV and 520 MeV were used.

The first target assembly consisted of two cylindrical thin aluminum flasks 11 inches long, 5 inches in diameter, with walls .0055 inches thick mounted one above the other. Their axes were along the ($\gamma = 0^{\circ}$) polarized beam line. They could be filled with hydrogen and deuterium respectively.

The entire target vacuum jacket was raised or lowered to put one flask or the other into the beam. This allowed rapid changes between neutron and proton polarized beams, for checks for experimental bias or malfunction.

An elastic scatter was chosen by requiring a recoil proton at roughly the correct angle to be counted in a hodoscope T, (see Fig. 3) consisting of six pairs of scintillators 3" x 8" x 1/4", viewed by 1P21 photomultiplier tubes. A coincidence in any pair was the tag for the beam nucleon.

Removing the low-energy contamination from the polarized beam by using a hodoscope to detect the recoil proton was deemed necessary because the lower-energy nucleon-nucleon cross sections are large. Typical energy distributions for a proton and a neutron beam with and without the hodoscope are shown in Fig. 4. Full-width-at-half-maximum of the proton distribution is 40 MeV; that of the neutron distribution is 50 MeV.

The average angle γ of the unpolarized beam was determined by two 6" x 6" split ion chambers, mounted on the upstream and downstream ends of an arm pivoted about the center of the target. Magnets B1 and B2 were tuned to center the beam on both split ion chambers.

Since the polarized beams made by scattering at positive and negative angles γ are assumed to have polarizations of equal magnitude but opposite orientation, the actual equality of the angles was checked both by transit measurement, and by comparing the energy distributions of the two beams with spectrometer B4 set in the polarized beam at $\theta_3=0^\circ$. The energy distributions were equal to within 3 ± 5 MeV, corresponding to a difference in laboratory scattering angle of $.2^\circ \pm .5^\circ$. For this angular error, the difference in polarization between the two beams would have been not more than $.004 \pm .008$. This uncertainty is much smaller than the statistical uncertainty in the measurement of the beam polarization.

C. Polarized Beam

The spins of the secondary beam nucleons could be precessed $\pm 90^{\circ}$ by a superconducting solenoid. It was necessary to undertake the design and fabrication of a superconducting magnet, since a conventional copper solenoid would have had to have been ten feet long in order to meet the half-megawatt power limitation imposed by available power supplies. Such a length would have decreased the solid angle subtended by the second target, and thus the rate, intolerably.

The solenoid consisted of 39,000 turns of 52% Nb-48%Ti wire, wound in three sections for convenience. It had a warm bore aperture of 4-1/4 inches. The coil was three feet long with an inside diameter of 5.2 inches.[13] These dimensions lead to a field configuration which has considerable variations over the entire aperture from that of an infinite solenoid. Since radial-field end effects do not cancel unless the spin precession is $2n\pi$ (n an integer), additional windings were placed on the ends of the coils to decrease the ratio $\int B_\rho dz / \int B_z dz$ through each end region, and thus to lessen the polarization structure in the direction of the momentum vector of the beam. Line integrals $\int B_z dz$ were measured as functions of current and radius to .1% accuracy.

Inductance of the coil was measured to be 35 Henrys. Changing the polarity of the field typically took 30 minutes. Bringing the magnet to full current more quickly might have been possible. However, increasing dB/dt increases the chance of driving the coil normal. Recooling and retransfering helium required several hours, and the probability of a winding slippage during transition was unknown. Since the magnet was buried in an 18-foot-thick shielding wall, conservatism prevailed.

A 9" x 12" C magnet, B3, was placed downstream of the solenoid to sweep charged particles below the beam line when a polarized neutron beam was desired. When the neutron beam polarization was vertical as for D measurements, the sweeping magnet B3 precessed the spin by about 20° into the direction of the momentum vector.

Thus the polarized beam which impinged on the second target could have its spin aligned in four directions, ("up", "down", "left", "right") with two combinations of angle γ and solenoid current possible for the "left" and "right" orientations. Table 1 shows polarizations and intensities of all beams used.

D. Second Scatter

The experimental apparatus for selecting events scattered from the polarized beam and analyzing the polarization of the outgoing proton is shown in Fig. 5.

The second target was a thin-walled mylar cylindrical flask filled with liquid hydrogen. The axis was along the polarized-beam line. It had length 12" and diameter 6".

In the study of proton-proton interactions, one proton is counted in scintillator Rec with its scattering angle θ_4 measured by magnetostrictive spark chambers 1 and 2. A count in this scintillator is not required when neutron-proton interactions are studied, or when $\theta_3 = 0^{\circ}$.

The proton momentum and scattering angle θ_3 are measured by the spectrometer magnet B4.

Magnetostrictive chambers 3-5 upstream of B4 determine the entrance angle to B4 and the front two or more chambers in the downstream array determine the exit angle. Magnet B4 was on a circular track and a pivot,

so various θ_3 ranging from 0° to 55° in the laboratory could be selected. Aperture was $\pm 5^\circ$ in the laboratory scattering angle. The momentum resolution was typically 2 or 3%. The magnet was run at low field to minimize dispersion, so that most of the particles entered the analyzing array of carbon slabs and spark chambers nearly normal. High resolution was not needed to distinguish elastic from inelastic events.

E. Third Scatter

The third scatter, which determines the polarization of the final state proton, takes place in an array of seven magnetostrictive spark chambers and four carbon slabs. The pairs of chambers on the upstream and downstream ends of the package had no carbon slabs between them, to measure the B4 spectrometer magnet exit angle, and to facilitate on-line monitoring of the scattering angle distribution in the carbon.

The magnetostrictive chambers[14] were single-gap chambers, consisting of two crossed planes of parallel .007 inch copper wires. Wire spacing was 1 mm. Gap width was 3/8". Sheets of aluminized mylar were placed on the outsides of the wire planes of the larger chambers to help carry ground current and decrease inductance. When a trigger occured, a .005 uf. capacitor charged to 6.5 kV was discharged into each chamber.

A 15% Helium - 85% Neon gas mixture mixed with approximately 1% ethanol vapor was recirculated through the chambers.

The chambers and carbon slabs increased in size from 14" x 18" active area, on the upstream side, to 28" x 32" on the downstream side, so that any proton scattered by 25° or less would not escape the trigger. Due to the relatively large spread in slopes of incoming particles, an anti-coincidence against small-angle scatters was not judged possible. Approximately 3% of the events recorded made a scatter within the angular

region $6^\circ < \theta_c < 22^\circ$. The third-scatter array was designed for this angular acceptance on the basis of known carbon analyzing power.[11]

No energy determination of the proton after the carbon scatter was attempted. Instead, all events, with elasticity undetermined, were used. Effective analyzing power for this selection of events was determined by placing the analyzing array in a beam of known polarization. Inelastic events are known to have lower analyzing power.[12] However, in this experiment, severely inelastic events were partially suppressed because the multiple scattering of the outgoing particle produced a poor fit to a single scatter hypothesis, or because more than one outgoing track came from the vertex. The observed effective analyzing power ranged between .26 and .48, as shown in Fig. 6.

The rate of triply-scattered events ranged from 1 per second for θ_3 small, to 1 per 25 seconds for θ_3 large.

F. Fast Electronics

Four scintillation counters monitored the polarized beam: M1, the passive sum of signals from two scintillators L1 and R1 counting the left and right halves of the beam, respectively; M2, a circular scintillator directly in front of the target counting only those particles passing into the target; and M3, a scintillator with a circular hole the size of the desired aperture, in anticoincidence. All M scintillation counters were viewed by Amperex 56AVP phototubes with additional current supplied to the last few dynodes to handle the several-megacycle counting rate.

For a polarized proton beam, the coincidence $M = M_1 M_2 \overline{M}_3$ was required. When a polarized neutron beam was run, the requirement was that no beam scintillator count: $\overline{M} = \sum_{i=1}^{4} M_i$.

The proton scattered from the second target was detected by coincidence $S = S_1 \bar{S}_2 S_3 S_4$. S_1 was in front of the momentum-analyzing magnet as was pole-tip anti S_2. S_3 and S_4 were passive sums of signals from pairs of scintillators upstream and downstream of the carbon target. The S counters were viewed by RCA 6810A phototubes. They were carefully tested for uniform efficiency.

At small lab angle θ_3 numerous deuterons are produced from the reaction $pp \rightarrow \pi d$, and it was possible to reject these from the trigger by their longer time of flight along the path between S_1 and S_4.

The tagging hodoscope T detected the recoil proton from the elastic scatter at the first target. A coincidence in any pair of hodoscope scintillators was required for a trigger. The MS signal was also fed into these coincidence circuits to keep the rate of output pulses lower. For a polarized proton beam, the Rec scintillator was also put into coincidence to tag the conjugate proton. Careful clipping of all counter signals and coincidence outputs was done to minimize accidentals.

G. Data Acquisition

After voltage was applied to the spark chambers and sparks occured, the wand signals were digitized by the magnetostrictive scalers and were strobed into a data buffer in a PDP-5 computer. When the buffer was filled with 23 events, it was written on magnetic tape. On-line monitoring of all chamber efficiencies and displays of reconstructed events were done. Various numbers of interest were typed out after each run was completed.

IV. DATA ANALYSIS

A. Pattern Recognition

Straight-through tracks in the analyzing-array spark chambers were identified from the table of 14 spark coordinates by counting the number of sparks within a small corridor along a line connecting the spark in the first chamber to the spark in the last. If 13 or 14 spark coordinates lay along the line, the event was discarded as a straight-through. Scatters of less than three degrees were nearly always identified as straight-through. About 90% of the events on magnetic tape had such small-angle scattering in the carbon. Straight-through events were used to check relative alignment of the chambers at frequent intervals during the running. Programs were designed to handle records with two tracks in the back chambers, but few were observed.

If an event was not identified as a straight-through, the straight segments of the track were identified by a similar method to that described above, and the approximate vertex position found by determining the intersection of the segments. Then a least-squares fit was performed, with the x (horizontal) and y (vertical) incoming and outgoing slopes, as well as the z coordinate of the vertex as variables. Since the efficiency of the chambers had to be high in order not to introduce possible geometrical bias, there were usually 14 data points for a 5 parameter fit. The scattering angle θ_c and the polar angle ϕ were calculated.

Although the chambers rarely had missing sparks, the probability of properly reconstructing a scatter was not 100%. A compromise had to be made in setting the search corridor width. A narrow width is necessary to avoid assigning sparks near the vertex to the wrong segment when the scattering angle is small. A larger search corridor insures that large-angle scatters are observed, since sparks tend to drift away from the

particle trajectory when the angle of incidence on the chamber gap is large.

There are more small-angle scatters than large, therefore the search corridor was set small.

Resolution of the scattering angle θ_c was approximately proportional to θ_c due to the uncertainty in z coordinate of the vertex, and was $.3^\circ$ for $\theta_c = 6^\circ$, and 1° for $\theta_c = 22^\circ$.

B. Kinematic Reconstruction

If an event made a carbon scatter of $6^\circ < \theta_c < 22^\circ$, the momentum of the proton was then determined from the bend angle in the spectrometer. The missing mass was calculated and was required to be $< (m_p + m_\pi)$. With the neutron beam, additional more stringent cuts were made on the reconstructed kinetic energy of the polarized beam particle, calculated from the resolution of scattering angle θ_3, outgoing proton momentum and measured polarized-beam energy distribution. This was necessary since part of the halo of the beam grazed a portion of the target support structure, and scattered off heavy atoms.

When both final state particles were charged, the vertex position was required to be inside the target volume, and the opening angle to be correct for elastic scattering. With one neutron and one proton in the final state, the proton ray was required to have crossed the geometric center line of the beam within the target.

C. Asymmetry Determination

Those events surviving the elasticity cuts and having scattering

angle $6^{\circ} < \theta_c < 22^{\circ}$ were placed into one of 20 bins in polar angle ϕ. The distribution in ϕ was fit to

$$N(\phi) = N_o \left(1 + \epsilon \cos \phi + \delta \sin \phi\right) \tag{3.1}$$

with a least-squares fit.

Two other parameters were also used in the fit: α_x and α_y, the probability of not detecting a scatter in the x or y view, respectively. The introduction of these two additional variables improved the χ^2 of the fit, but did not affect the values found for ϵ and δ. See Appendix 1 for a more detailed discussion.

In the runs where the beam was polarized vertically, δ gives a measure of experimental bias, and $\epsilon = P_3 A$. P_3 is the polarization of the out-going proton from the second scatter, and A is here the effective analyzing power of the carbon.

The effective analyzing power of the carbon was measured by placing the carbon package in a proton beam of known polarization. The analyzing power was determined at seven energies between 200 MeV and 670 MeV. For energies lower than 520 MeV, copper degrader was placed in the polarized beam directly behind the first target.

The calibrating-beam polarization was determined by scattering at equal angles from the first and second targets. The beam intensity was lowered to keep the accidental rate below 1% for the calibration runs.

If N^+ is the number of scatters per unit beam intensity with positive first-scattering angle γ and N^- the same for negative γ, then

$$\frac{N^+ - N^-}{N^+ + N^-} = P(E_1)\, P(E_2) \tag{3.2}$$

where E_1 and E_2 are the energies of the first and second scatters, respectively. The relative energy dependence $P(E_1)/P(E_2)$ of the polarization was taken from the literature.[11]

D. Depolarization Parameter Calculation

From the definition of D in Fig. 1.

$$\epsilon_{RL} = AP_3 = \frac{A\left(P_2 + DP_1\right)}{1+P_1P_2} \tag{3.3}$$

where P_1 is the beam polarization, P_2 is the polarization observed if the initial beam is unpolarized, and A here is the effective analyzing power of carbon.

By taking data at positive and negative angles γ we may calculate

$$D = \frac{\left(\epsilon^{+}_{RL} - \epsilon^{-}_{RL}\right)}{2\ AP_1} \frac{\left(1 + P_1P_2\right)}{} \tag{3.4}$$

where superscripts indicate the sign of the angle γ. The product P_1P_2 is determined for each experimental setting of γ and θ_3 by comparing the number of elastic events going into the S channel per unit beam intensity for positive γ and negative γ.

$$P_1P_2 = \frac{N^{+}-N^{-}}{N^{+}+N^{-}} \tag{3.5}$$

P_1 for all proton beams is determined in the same way as for the analyzing-power-calibration beam. The technique for neutron beams must be different however, since doing equal angle scatters at the first and second targets requires the undesirable assumption that the neutron is free within the deuteron. Instead, the product P_1P_2 is measured as above, and P_2 is determined from the carbon right-left asymmetry in those runs where the polarization direction of the incoming neutron beam is horizontal. (The polarization of the beam in the plane of scattering does not contribute to the left-right asymmetry. Only P_2 contributes.)

V. RESULTS

A. Depolarization in the Proton-Proton System

Although at least six other D_{pp} experiments have now been performed in the energy range 425-660 MeV, it was felt that the experimental picture was still cloudy enough to merit more work. Fig. 7 shows the wide scatter in the data accumulated after 1960 and before this work. Performing the D_{pp} experiment also allowed a valuable tuneup period before beginning the more difficult D^t_{np} run.

The values observed in this experiment are shown in Fig. 8, as well as in Table 2. Data at 520 MeV, 600 MeV, and 670 MeV were taken. Although the ratio of inelastic to elastic scattering goes from 10% at 425 to 40% at 650 MeV[21] we observe little change in the shape or magnitude of D_{pp} over this energy region. The solid line in Fig. 8 is the calculated value of D_{pp} at 500 MeV predicted by the Livermore energy-dependent phase-shift analysis.[22] The dashed lines indicate the error corridor. This extrapolation is made from the analysis of 1076 pieces of proton-proton data in the energy range 0 - 450 MeV. This prediction was not available for CM angles greater than 90°. The dotted line is a portion of a preliminary prediction from a similar Livermore analysis done earlier on pp data from 0 - 500 MeV. The predictions of both Livermore efforts seem to indicate the essential features of the data. The decrease in D_{pp} at angles larger than 90° CM seems more precipitious than predicted.

Several energy-independent phase shift analyses have been done in the neighborhood of 650 MeV. In Fig. 9 the solid line shows the solution for D_{pp} generated from the 660 MeV phase shift set obtained by the Kyoto group.[23] Their phase shift analysis was based on elastic differential cross-section, polarization, depolarization, and $C_{NN}(90^\circ)$ and $C_{KP}(90^\circ)$ data. Imaginary phase shifts were estimated by assuming that Δ (1236)

production dominates the inelastic scattering. Experimental points which were part of the input data are displayed together with the 670 MeV data of this work. The dashed line is from another Kyoto solution quoted by Roth et al.[15] The differences between the two solutions do not manifest themselves in the D_{pp} values.

The phase shift analysis done by Glonti et al (Dubna 1967)[24] yields the two calculated curves shown in Fig. 10. Also plotted are the D_{pp} data which were input to the analysis; a single point done by Bourquin et al at CERN,[16] two recent points from the Czechoslovakia group at Dubna[20] and the 600 MeV data of the present work. It seems clear that the more recent data tends to exhibit a lower value of D_{pp} at angles greater than 90°. The high statistics points near 60° CM of CERN and Dubna are in vast disagreement. Data of the present work does not resolve the conflict.

B. Transfer Depolarization in the Neutron-Proton System

The transfer depolarization in the neutron-proton system was measured by scattering polarized neutrons off hydrogen. Thus interpretation of the data is not complicated by requiring assumptions about the nature of the deuteron binding.

The D^{t}_{np} data taken at 520 MeV and 600 MeV are shown in Figs. 11 and 12. The dashed curve, shown with its error corridors, is a prediction by the Livermore group.[22] This extrapolation was done from an energy-dependent phase shift set computed from 990 pieces of np data from 0 - 450 MeV. The ^3S, ^3D mixing parameter ϵ_1 was constrained to be positive at energies in the neighborhood of 50 MeV. The solid curve is calculated from a phase shift set generated from the same np data with no restriction on the sign of the ϵ_1 term.

Neither prediction is overwhelmingly supported by the data as shown. However only one point lies more than two standard deviations away from the prediction which was generated assuming no restrictions on ϵ_1.

C. Contributions to Errors

In measuring D, equal time was spent accumulating data with the beam polarization positive and negative.

$$\epsilon^+ = P_3^+ A = (P_2 + DP_1)$$

$$\epsilon^- = P_3^- A = (P_2 - DP_1)$$

Solving for D in terms of the asymmetries,

$$D = \frac{(\epsilon^+ - \epsilon^-)\ (1 + P_1 P_2)}{2AP_1}$$

As discussed earlier, the variables measured in a determination of D are ϵ^+, ϵ^-, A, P_1 and the product $(P_1 P_2)$. Since $|P_1 P_2|$ is usually less than .2, the relative error on the term $(1 + P_1 P_2)$ is not a major contributor to the total error. The proton beam polarization had a relative statistical uncertainty of 2% - 5%, and the effective analyzing power of the carbon has 5% - 10% statistical error. The major contributions to the errors arise from the statistical uncertainties in ϵ^+ and ϵ^-. Stringent cuts on the momentum of the proton scattered from the second target were made to insure a cleaner but smaller sample of elastic events, since it was noticed that inelastic contamination gave an apparent D_{pp} much smaller than the true D_{pp}. In the neutron data, as many as 3/4 of the triply scattered events were rejected as inelastic. Most of these events were not connected with pion production in the hydrogen but with other inelastic processes induced in the target walls, the M2 scintillation counter, and

part of the target support by the halo of the neutron beam.

Checks against systematic errors were continuously employed during the running of the experiment. The first scattering angle δ was reversed often, to change the orientation of the polarization. Both possible combinations of solenoid polarity and sign of the first-scattering angle were used to prepare the beam with spin "right" and "left". In cases where there was no initial beam polarization in the plane of scattering, the up-down asymmetry, which is expected to be zero, was used as a monitor of false asymmetry in the third scatter.

The ratio of reconstructed elastic events per unit beam with target full to those with target empty was approximately 1000 for the polarized proton beam, and approximately 20 for the polarized neutron beam. Corrections were done in the standard fashion.

Besides the D and D^t parameters reported in this work, the experiment also measured R and R' for both the np and pp systems. These data will be reported in the dissertation of K. C. Leung. Data was taken to allow calculation of P_1 and P_2 for the np scattering. These values will also be reported by Leung. In the calculation of D^t_{np} in this work the values of P_1 and P_2 were taken from a polarization experiment by D. Cheng,[11] which was similar in beam design to this one. This was considered a reasonable approximation since the proton polarization measurements agreed extremely well between this experiment and that of Cheng. Although the author indicated errors on P_1 and P_2 of typically 5% - 8%, errors of 10% were included in this analysis, to indicate to the reader the size of the error bar of the expected final result.

D. Conclusion

Although many nucleon-nucleon experiments have been done in the

range of this experiment, many more need to be done, both to acquire additional new information and to resolve differences between existing experiments.

This experiment used a short, high field superconducting magnet to precess the polarized-beam-nucleon spin by $\pi/2$. It is felt that a superconducting solenoid with $\int B_z dz$ twice as large would be relatively easy to design and build, and would be extremely useful in future nucleon-nucleon studies. It would be particularly interesting to measure C_{NN} in the np system, so that the amplitudes $|f|^2$ and $|g|^2$ could be calculated for both I=0 and I=1.

ACKNOWLEDGEMENTS

It is a pleasure to thank my research director Leroy T. Kerth for encouragement, guidance and friendship throughout my graduate years and for his contribution to the success of this work. I would also like to thank K. C. Leung, who, as the other graduate student working on this project, participated in all phases of design, execution and analysis of the experiment. I am grateful to David Cheng and Burns MacDonald for contributions to designing and running the experiment. C. M. Ankenbrandt was a helpful contributor to the analysis programming. Malcolm MacGregor generously provided us extrapolated predictions from the Livermore energy-dependent phase shift analysis, before publication.

The 184" Cyclotron crew and the accelerator technicians provided a dependable proton beam and inexhaustable patience with this green graduate student during the setting up and running of the experiment. Other excellent support groups in various shops and in the computer center, as well as the Lofgren Physics group technicians, expedited the project.

My thanks also go to Michael Barnes for help with data handling, and to William Forsythe for help during the early stages of the work.

I am especially grateful to my husband Clifford, and my children Michael and Leslie, who have put up with several years of irregular dinner hours, dusty furniture, and unmated socks with cheerfulness and good grace. This work could not have been completed without their loving patience and active support.

This work was done under the auspices of the U. S. Atomic Energy Commission.

APPENDIX 1

Polar Angle Efficiency Correction

With the pattern-recognition program described in Chapter IV, the probability of missing a projected scatter θ_x or θ_y is 1 when θ_x or θ_y is less than 3°. If the probability for missing a larger angle scatter is α, then in the shaded region of Fig. A1, the probability for missing the scatter in both views is

$$P_{miss} = P_x P_y = 1.(\alpha) = \alpha \tag{A1}$$

In the unshaded regions, both views of the scattered event show angles larger than 3°, and so

$$P_{miss} = P_x P_y = (\alpha)(\alpha) = \alpha^2 \tag{A2}$$

Since α is less than 1, the probability of missing an event is greater along the x and y axes. This detection inefficiency would make a flat phi distribution show dips around $\Phi = 0^\circ, \pm 90^\circ, 180^\circ$.

In practice, an independent efficiency parameter depending linearly on the projected scattering angle, was used for each view.

Making this type of efficiency correction improves the X^2 for a fit to $A(1 + \epsilon \cos\Phi + \delta \sin\Phi)$ but does not affect the values attained for ϵ and δ.

For example, suppose R events are in the $\Phi = 0^\circ$ bin and L events are in the $\Phi = 180^\circ$ bin. Other bins are empty. Suppose a fraction α_x are not observed. Then

$$\epsilon_{apparent} = \frac{R(1 - \alpha_x) - L(1 - \alpha_x)}{R(1 - \alpha_x) + L(1 - \alpha_x)} = \epsilon_{true}$$

REFERENCES

1. L. Wolfenstein and J. Ashkin, Phys. Rev. 85, 947 (1952).

2. R. H. Dalitz, Proc. Phys. Soc. A65, 175 (1952).

3. M. J. Moravcsik, Two-Nucleon Interaction (Oxford University Press, 1963).

4. For a detailed discussion see: H. F. Stapp, Thesis, University of California, Lawrence Radiation Laboratory Report UCRL-3098 (1955).

5. L. Wolfenstein, Ann. Rev. Nucl. Sci. 6, 43 (1956).

6. S. M. Bilenkii, L. I. Lapidus, and R. M. Ryndin, Soviet Physics JETP, 24, 3, 593 (March 1967).

7. L. D. Puzikov, R. M. Ryndin, Ya. A. Smorodinskii, Soviet Physics JETP, 5, 489 (1957).

8. C. R. Schumacher and H. A. Bethe, Phys. Rev. 121, 5, 1534 (1961).

9. M. H. MacGregor, R. A. Arndt, and R. M. Wright, Phys. Rev. 182, 5, 1715 (1969).

10. M. L. Goldhaber in Proceedings of the Midwestern Conference on Theoretical Physics (Purdue University. Lafayette, Ind. April 1960).

11. D. Cheng, Thesis, University of California, Lawrence Radiation Laboratory Report UCRL-11926 (1965).

12. W. A. McNeely, Jr., California Institute of Technology Report CALT 68-113 (1967).

13. More details on the magnet design may be found in: R. B. Meuser, W. H. Chamberlain, and R. E. Hintz, Lawrence Radiation Laboratory Report UCRL-18179 (1968).

14. For a discussion of similar magnetostrictive chambers see: V. Perez-Mendez, Lawrence Radiation Laboratory Report UCRL-17121 (1966).

15. R. Roth, E. Engels et al., Phys. Rev. 140, 6B, B1533 (1965).

16. M. Bourquin et al., Helv. Phys. Acta 39, 579 (1966).

17. Yu. M. Kazarinov et al., RMP, 39, 509 (1967).

18. Yu. M. Kumekin, M. G. Meshcheryakov, S. B. Nurushev, and G. D. Stoletov; JETP, 38, 1451 (1960). Correction by L. S. Azhgirey et al., in Sov. J. Nuc. Phys. 2, 892 (1965).

19. R. Ya. Zulkarneev, V. S. Nadesdin and V. I. Salarov. Proceedings First Int. Colloquim on N-N and π-Interactions, (Dubna 1968) p. 88.

20. J. Bystricky, J. Čech, Z. Janout, Yu. M. Kazarinov, F. Lehar and L. B. Parfenov, Physics Letters, 28B, 8, 572 (1969).

21. M. H. MacGregor, Physics Today 22, 12, 21 (Dec. 1969).

22. M. H. MacGregor, Private communication. Extrapolation done from the work described in M. H. MacGregor, R. A. Arndt, and R. M. Wright, Phys. Rev. 182, 5, 1714 (1969).

23. Norio Hoshizaki and Shiagru Machida, Prog. Theor. Phys. 29, 1 (1963), Kyoto.

24. L. I. Glonti, Yu, M. Kazarinov, A. M. Rozanova and I. N. Silin Preprint JINR P1-3525, Dubna (1967).

25. For an excellent treatment of both the Wolfenstein and the helicity amplitude formalisms, see: P. D. Grannis, Lawrence Radiation Laboratory Report UCRL-16070.

TABLE 1

Polarized Beam Characteristics

Beam Type	γ	Kinetic Energy	Polarization	Intensity
p	$\pm 15^{\circ}$	670 ± 20 MeV	.51 ± .01	$2 \cdot 10^{6}$ protons/sec
p	$\pm 22^{\circ}$	600 ± 20 MeV	.53 ± .01	$1 \cdot 10^{6}$
p	$\pm 28^{\circ}$	520 ± 20 MeV	.43 ± .02	$1 \cdot 10^{6}$
n	$\pm 22^{\circ}$	600 ± 25 MeV	−.275 ± .022(*)	$4 \cdot 10^{5}$ neutrons/sec
n	$\pm 28^{\circ}$	520 ± 25 MeV	− .35 ± .026(*)	$3 \cdot 10^{5}$

Beam Cross Sectional Area: 28 in^2

(*) Values taken from D. Cheng, reference 11.

Table 2

	670 MeV		600 MeV		520 MeV	
θ_{cm}	P_1P_2	D_{pp}	P_1P_2	D_{pp}	P_1P_2	D_{pp}
$35^\circ \pm 10^\circ$	.256 ± .011	.61 ± .11	.305 ± .011	.84 ± .15	.228 ± .021	.55 ± .29
$58^\circ \pm 10^\circ$	.208 ± .018	.76 ± .14	.175 ± .013	.43 ± .16	.173 ± .015	.58 ± .35
$79^\circ \pm 10^\circ$	.148 ± .015	–	.042 ± .012	–	.055 ± .015	.77 ± .11
$99^\circ \pm 10^\circ$	–.046 ± .008	.70 ± .09	–.010 ± .008	.55 ± .08	.000 ± .017	.75 ± .09
$109^\circ \pm 10^\circ$	–.150 ± .010	.36 ± .04	–.116 ± .008	.37 ± .08	–.104 ± .008	.33 ± .11
$118^\circ \pm 10^\circ$	–.133 ± .011	.29 ± .15	–.162 ± .01	.14 ± .06	–.15 ± .05	.18 ± .07
	P_1 = .51 ± .01		P_1 = .53 ± .01		P_1 = .43 ± .02	

	600 MeV		520 MeV	
θ_{cm}	$P_2^{(*)}$	D^t_{np}	$P_2^{(*)}$	D^t_{np}
$65^\circ \pm 10^\circ$	.20 ± .03	.18 ± .21	–	–
$90^\circ \pm 10^\circ$	–.25 ± .03	.23 ± .30	–.24 ± .03	.12 ± .32
$102^\circ \pm 10^\circ$	–.34 ± .03	.58 ± .28	–.27 ± .03	–.04 ± .16
$124^\circ \pm 10^\circ$	–.30 ± .03	+.10 ± .43	–.21 ± .02	–.67 ± .29
$180^\circ \pm 10^\circ$	.0	–.05 ± .84	.0	.12 ± .33
	$P_1^{(*)}$ = .275 ± .022		$P_1^{(*)}$ = –.35 ± .026	

(*) Values taken from D. Cheng, reference 11.

FIGURE CAPTIONS

Fig. 1. Definition of Wolfenstein parameters.

Fig. 2. Schematic diagram of the experimental apparatus. In the drawing B_i represent bending magnets, T is a tagging hodoscope, M_i are beam monitor scintillation counters, and S_i are scintillation counters monitoring scattered particles. Spark chambers are numbered from 1 to 12.

Fig. 3. Detail of the apparatus used to produce a polarized beam.

Fig. 4 Illustration of typical energy distributions of proton and neutron beams, with and without tagging hodoscope T in the trigger.

Fig. 5. Detail of the experimental apparatus used to monitor the second and third scatters.

Fig. 6. Variation of effective analyzing power of the carbon target with kinetic energy.

Fig. 7. Data from earlier D_{pp} experiments, plotted against θ_{CM}.

Fig. 8. Comparison of our D_{pp} at 520 MeV, 600 MeV, and 670 MeV to the phase shift prediction of MacGregor[22] extrapolated to 500 MeV.

Fig. 9. The 670 MeV D_{pp} data of this work compared with the curve calculated by the Kyoto group[23] from an energy independent phase shift analysis at 660 MeV based on the data of Kumekin.[18]

Fig. 10. D_{pp} at 600 MeV compared with the calculated value from the Glonti phase shift set[24] and data from earlier experiments.

Fig. 11. Transfer depolarization in np scattering, D^t_{np}, at 520 MeV. The solid curve is an extrapolation to 500 MeV from the MacGregor[9] phase shift analysis, assuming no restrictions on ϵ_1. The dashed curve is from the same phase shift analysis,

with the restriction $\epsilon_1 > 0$

Fig. 12. D^t_{np} at 600 MeV. The MacGregor predictions are also plotted.

Fig. A1 Geometry for calculation of the polar angle efficiencies.

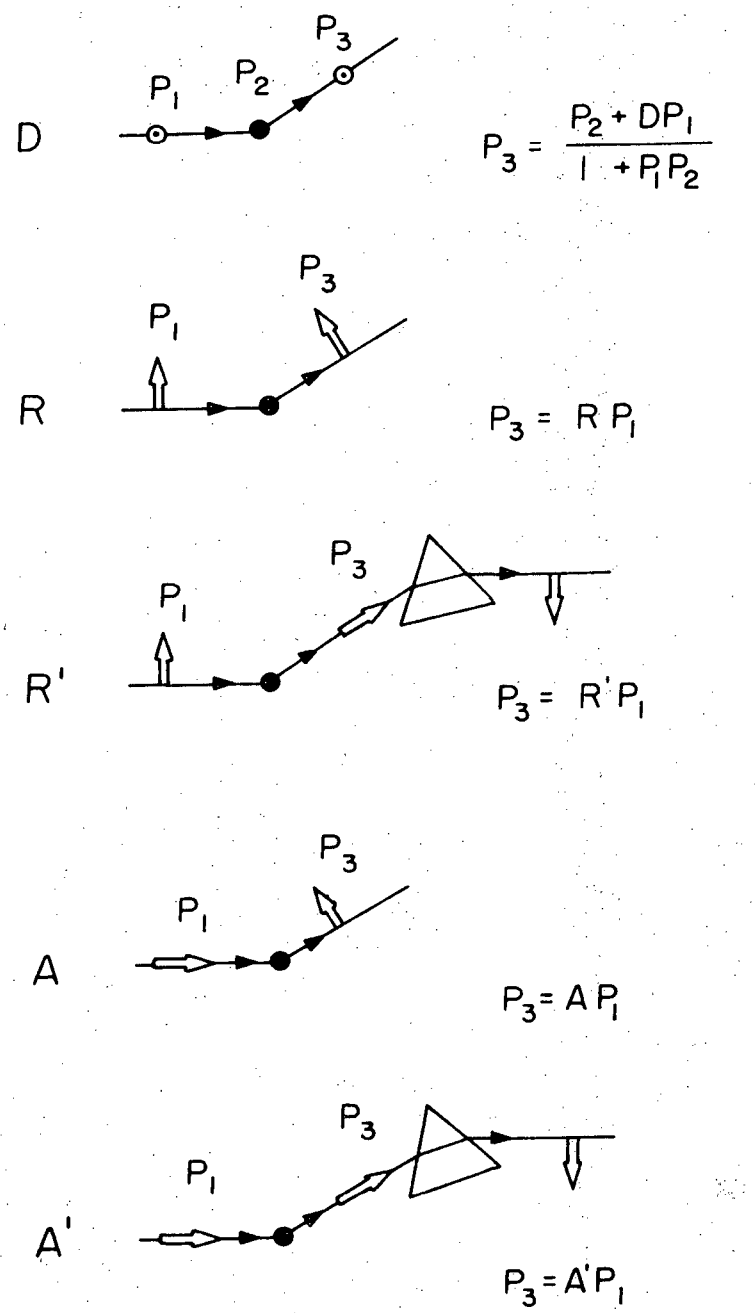

XBL 701-186

Fig. 1

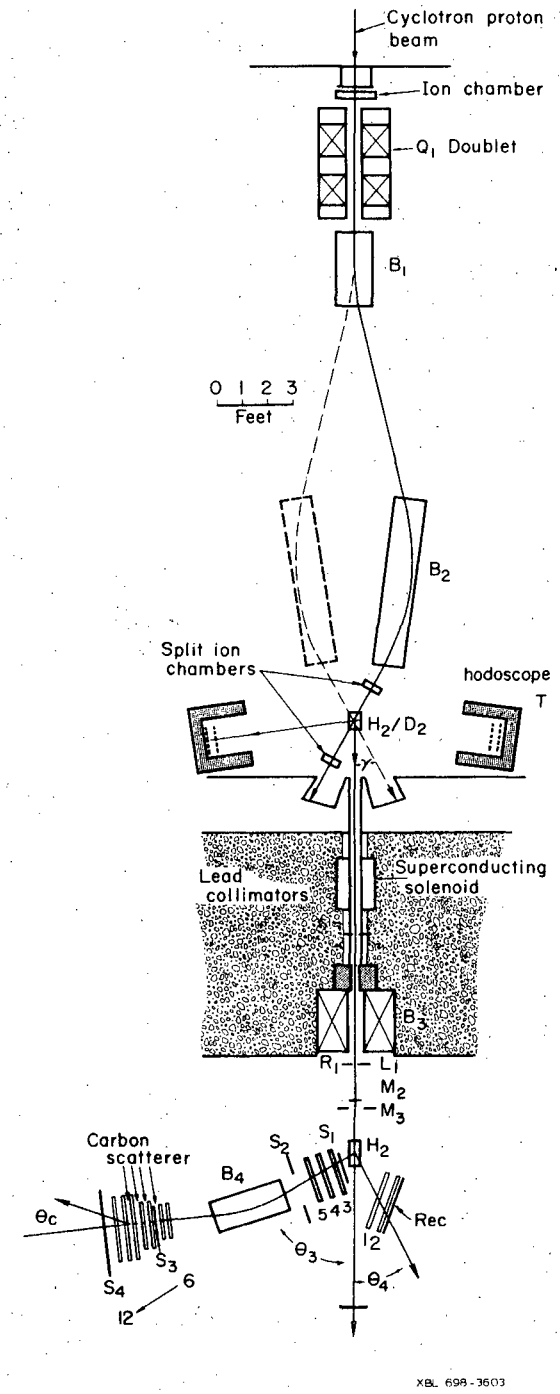
Cyclotron proton beam
Ion chamber
Q_1 Doublet
B_1
0 1 2 3
Feet
B_2
Split ion chambers
hodoscope
T
H_2/D_2
Lead collimators
Superconducting solenoid
B_3
R_1
L_1
M_2
M_3
Carbon scatterer
S_2
S_1
H_2
B_4
θ_c
5 4 3
Rec
12
θ_3
θ_4
S_3
S_4
6
12
XBL 698-3603

Fig. 2

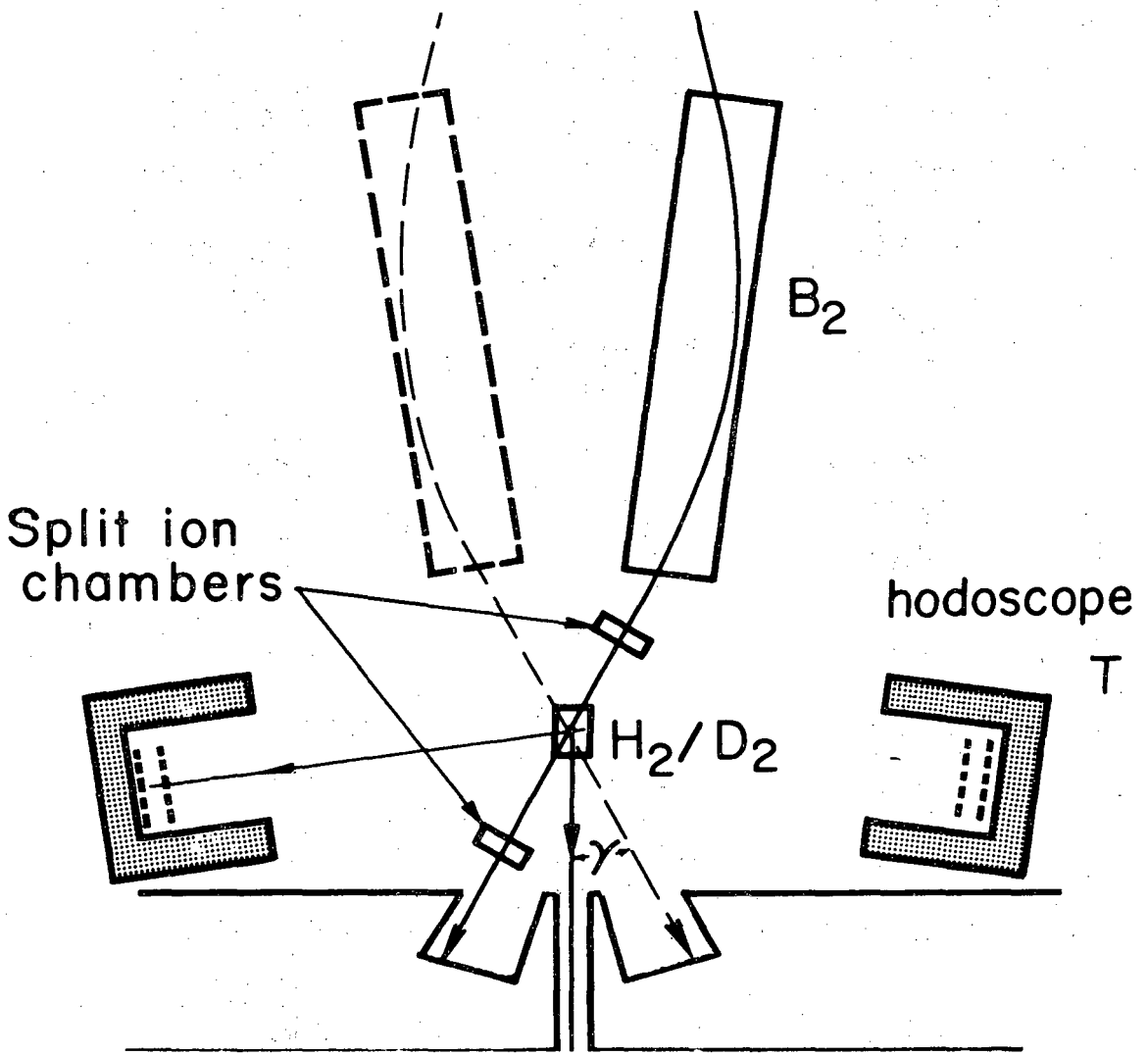

XBL 698-3603-A

Fig. 3

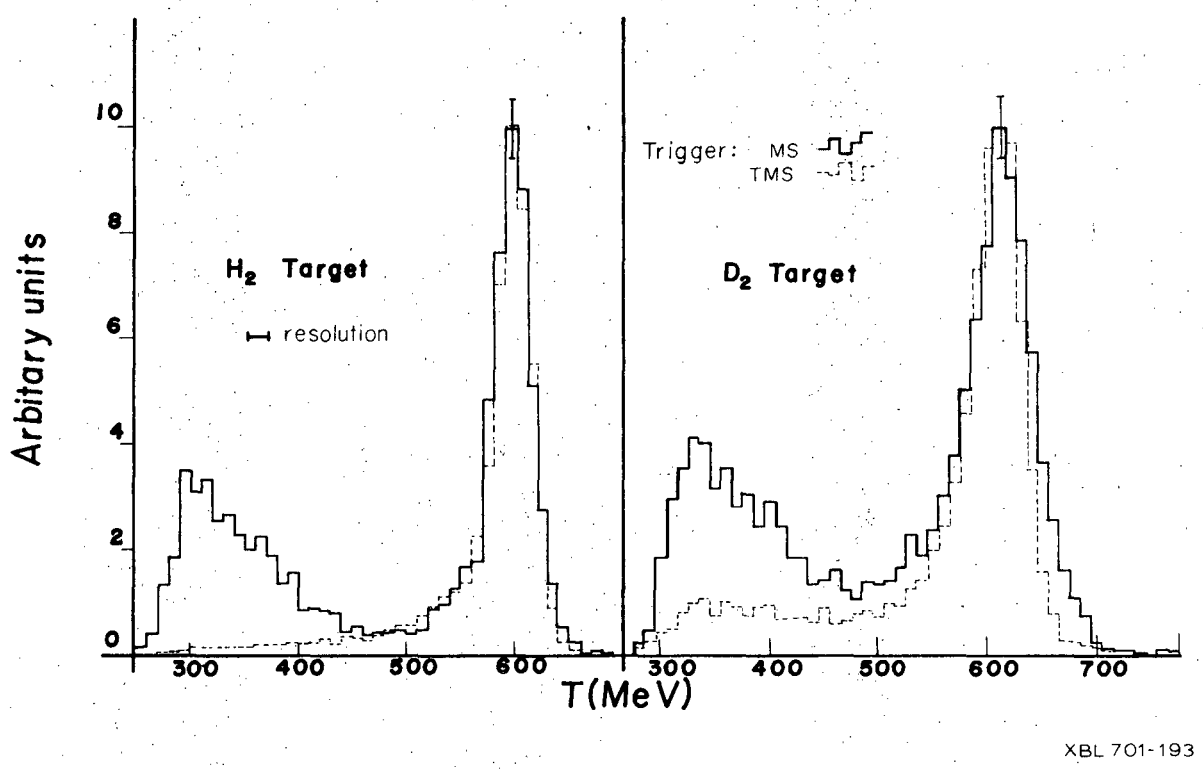
Arbitary units
10
8
6
4
2
0
H2 Target
resolution
D2 Target
Trigger: MS
TMS
300
400
500
600
700
T(MeV)
XBL 701-193

Fig. 4

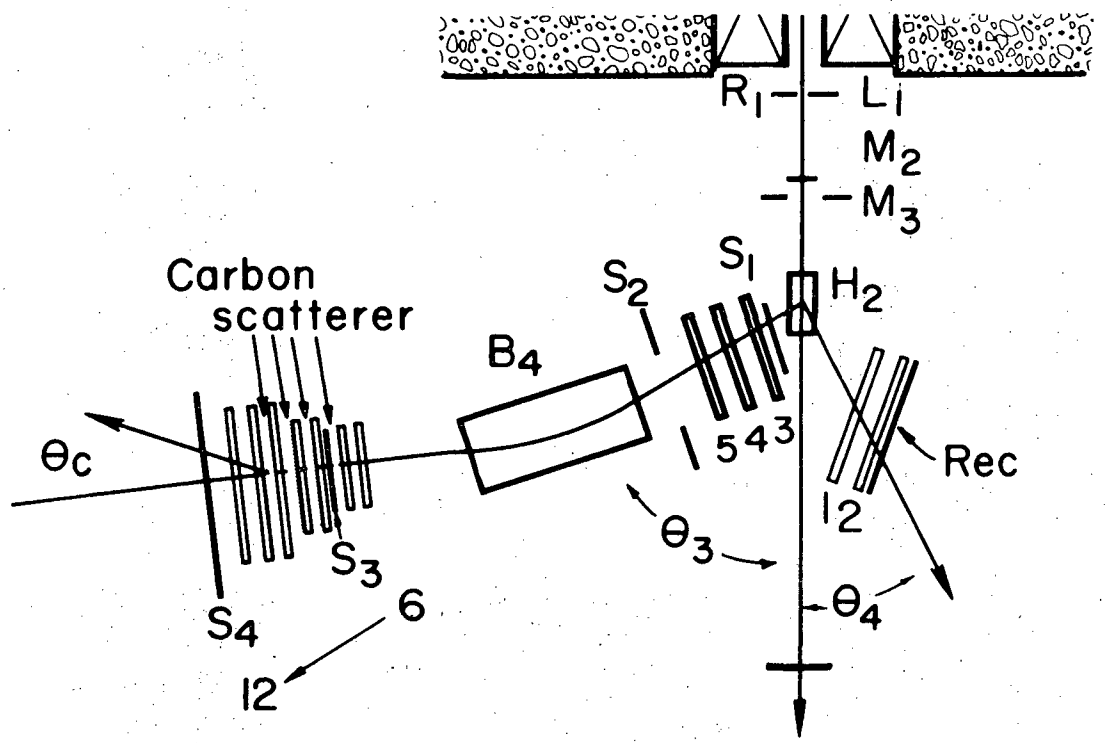

XBL 698-3603-B

Fig. 5

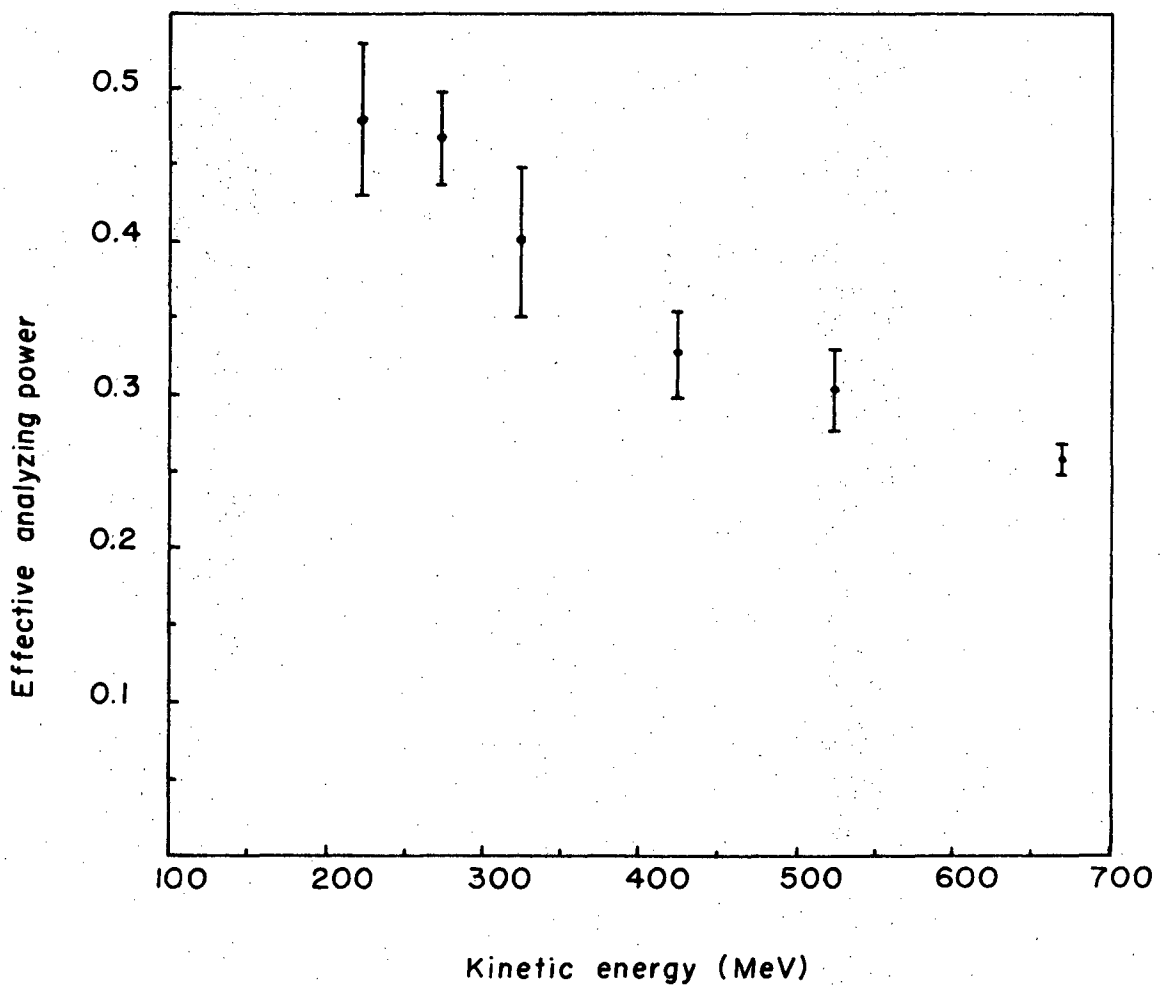

XBL 702-247

Fig. 6

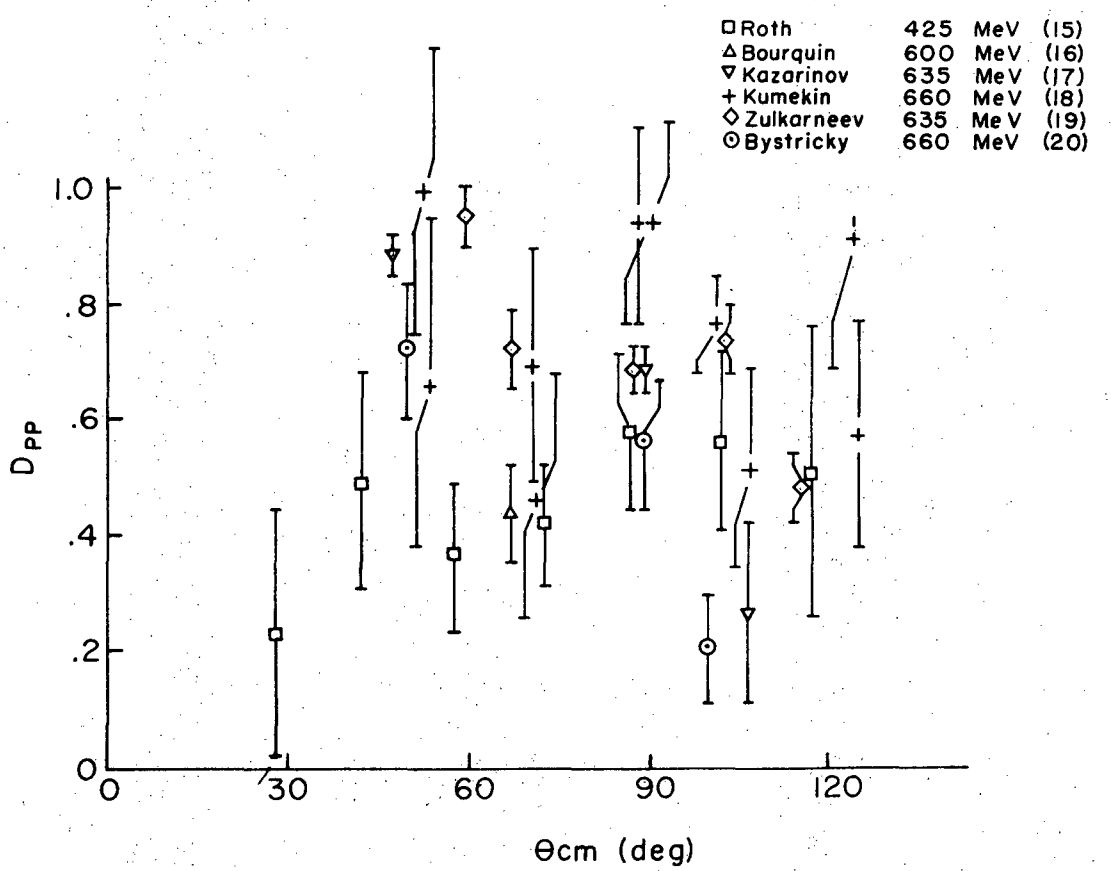

XBL 701-187

Fig. 7

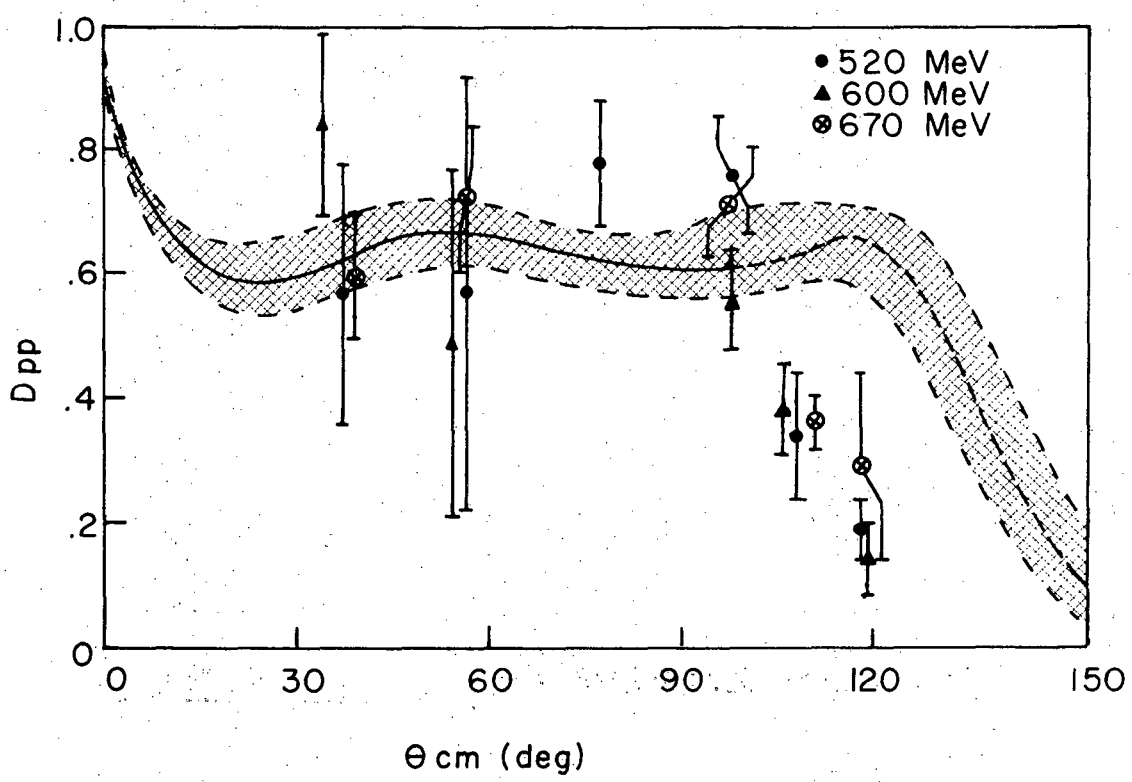

XBL 701-190

Fig. 8

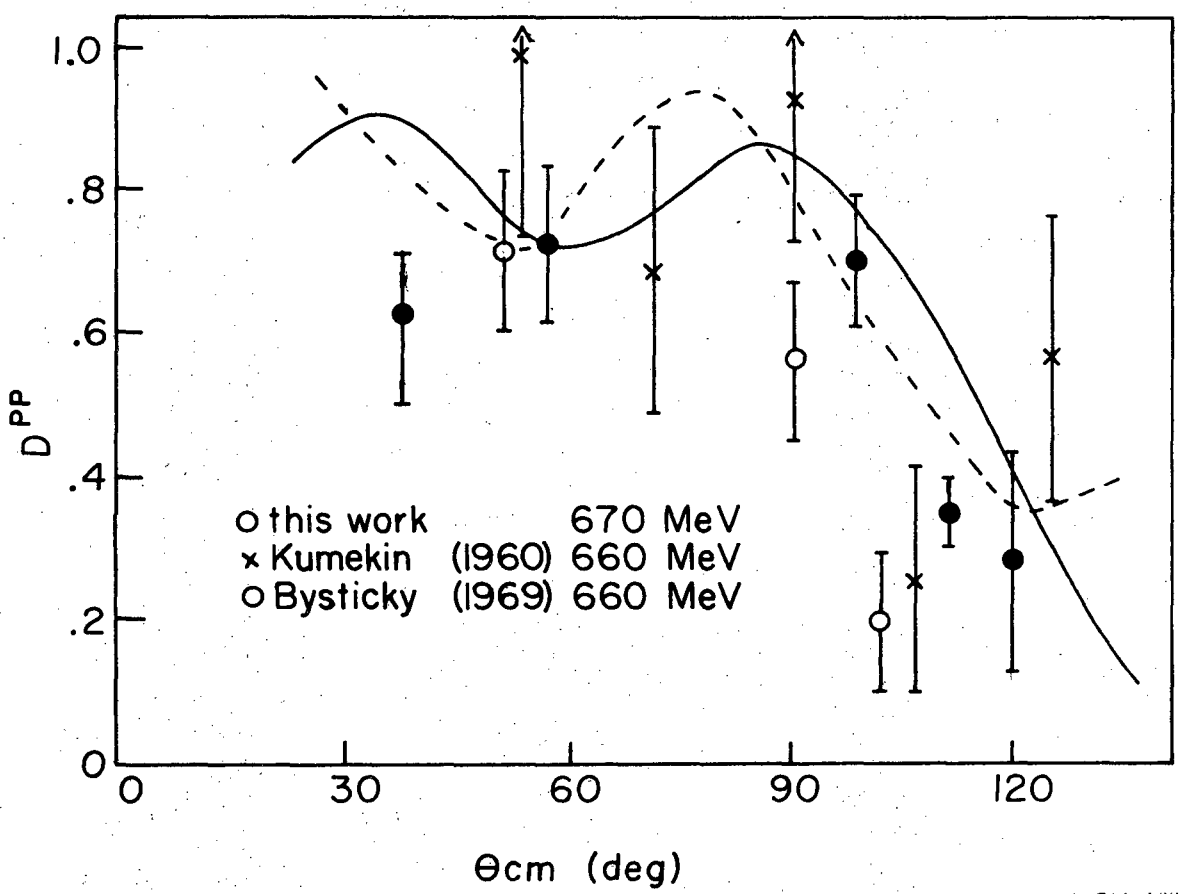

XBL 701-189

Fig. 9

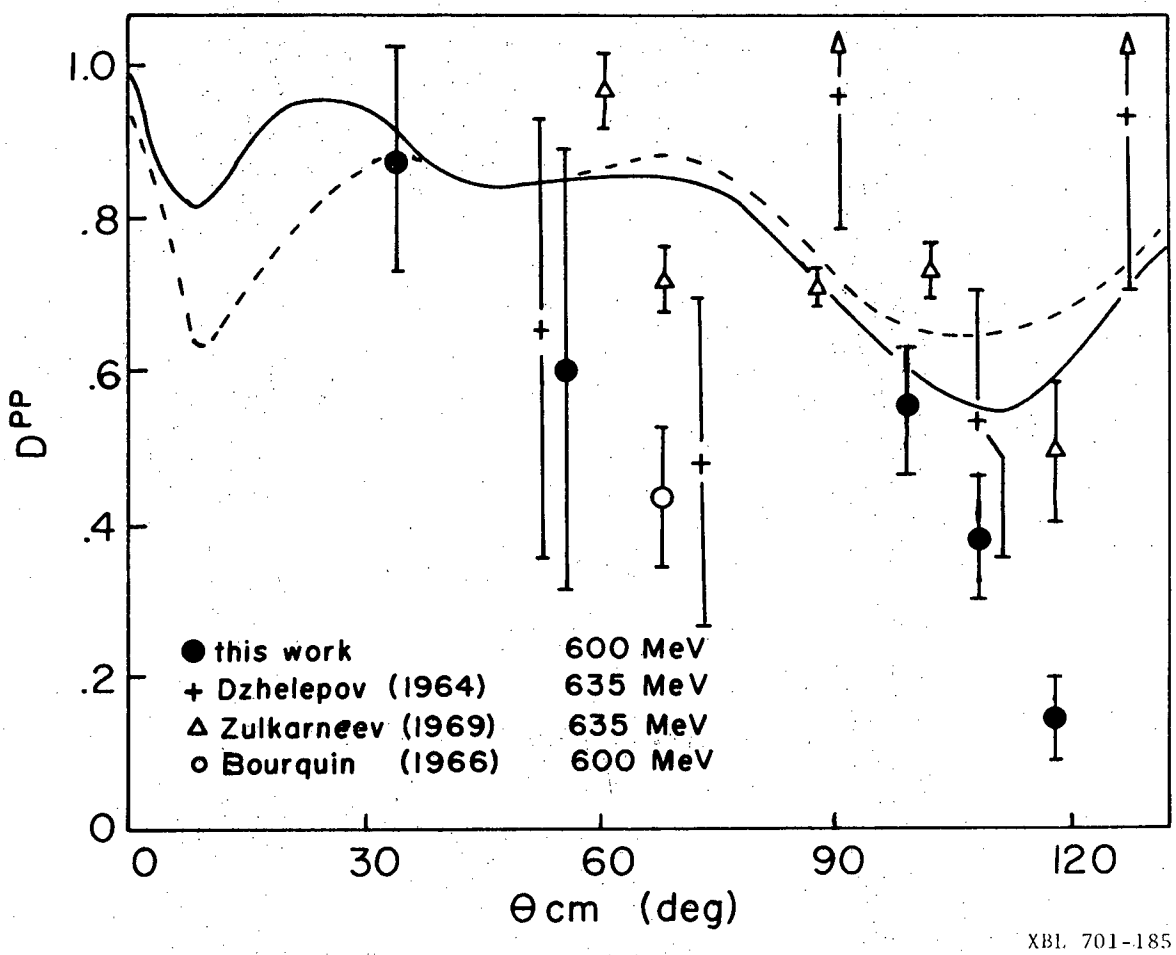

XBL 701-185

Fig. 10

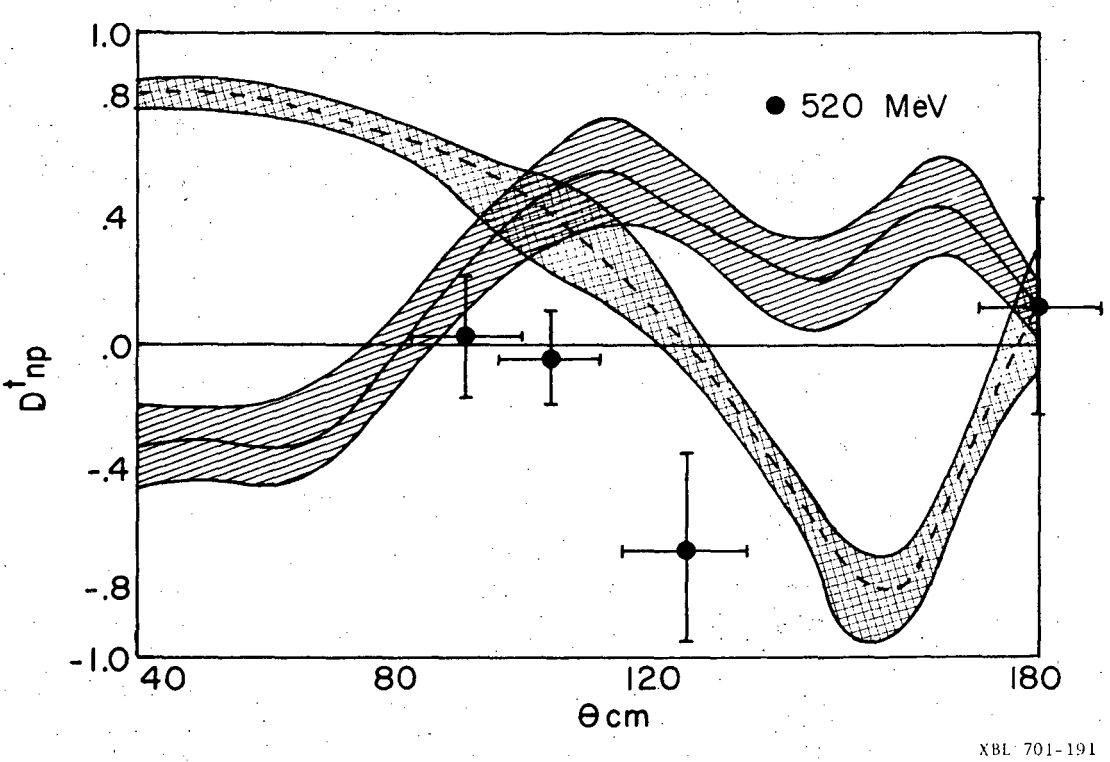

Fig. 11

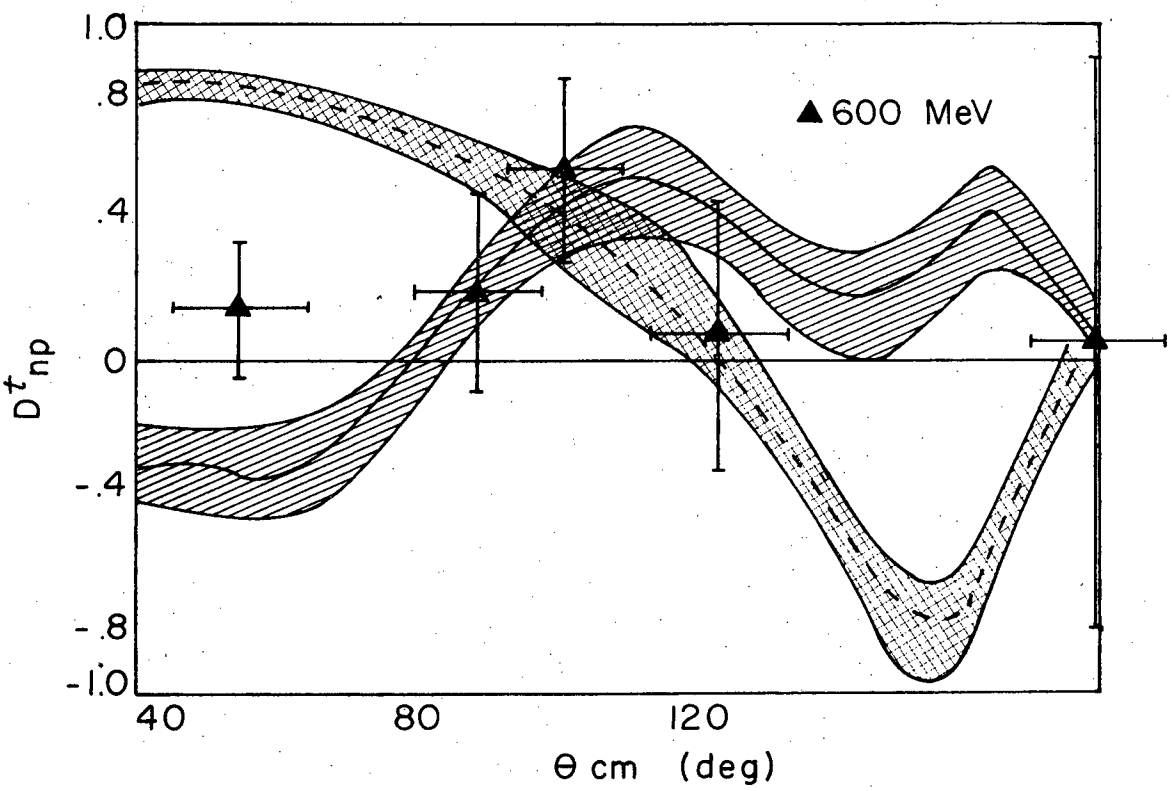

XBL 701-192

Fig. 12

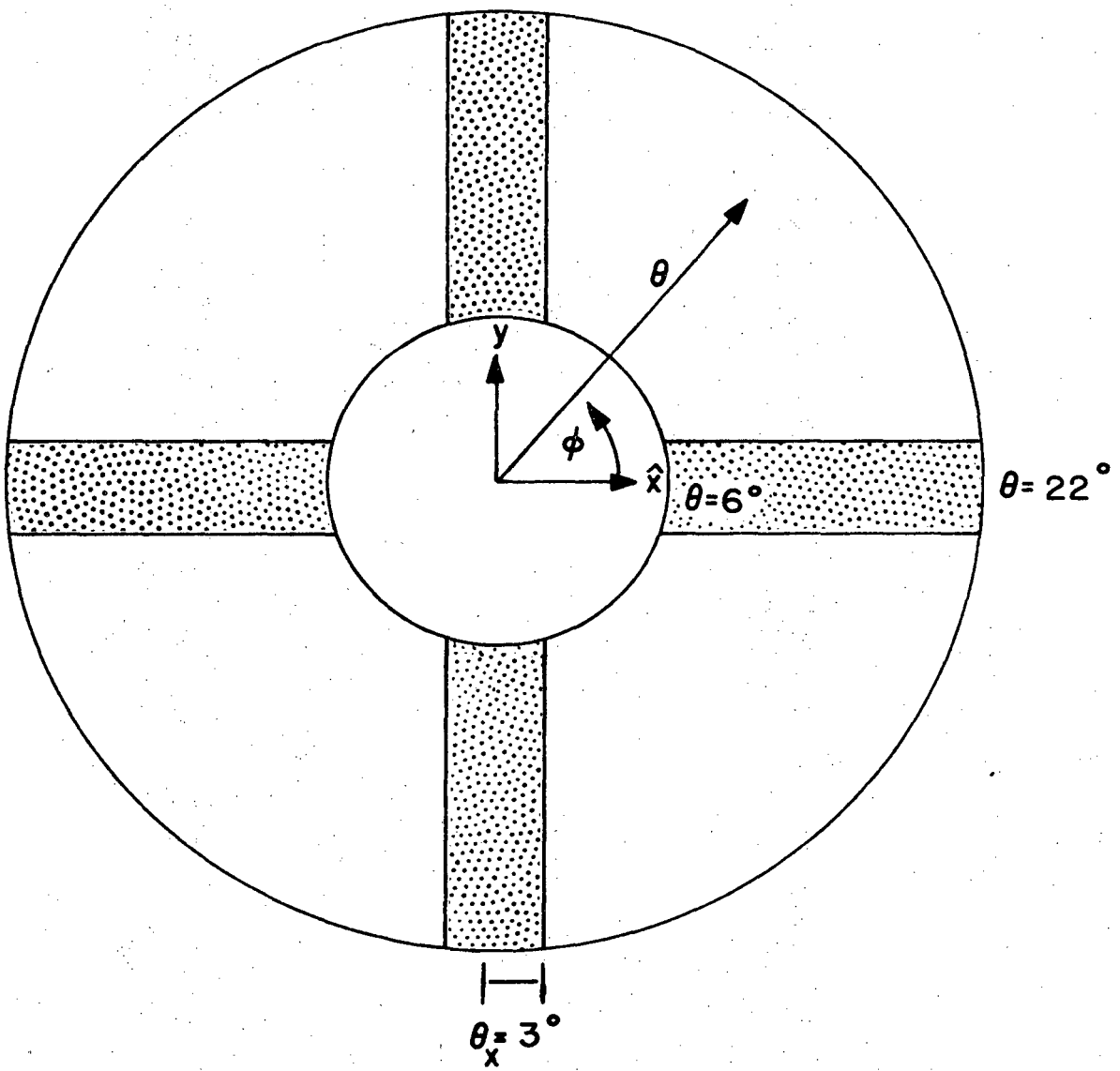

XBL 701-188

Fig. A1

LEGAL NOTICE

This report was prepared as an account of Government sponsored work. Neither the United States, nor the Commission, nor any person acting on behalf of the Commission:

A. Makes any warranty or representation, expressed or implied, with respect to the accuracy, completeness, or usefulness of the information contained in this report, or that the use of any information, apparatus, method, or process disclosed in this report may not infringe privately owned rights; or

B. Assumes any liabilities with respect to the use of, or for damages resulting from the use of any information, apparatus, method, or process disclosed in this report.

As used in the above, "person acting on behalf of the Commission" includes any employee or contractor of the Commission, or employee of such contractor, to the extent that such employee or contractor of the Commission, or employee of such contractor prepares, disseminates, or provides access to, any information pursuant to his employment or contract with the Commission, or his employment with such contractor.

TECHNICAL INFORMATION DIVISION
LAWRENCE RADIATION LABORATORY
UNIVERSITY OF CALIFORNIA
BERKELEY, CALIFORNIA 94720